Published in final edited form as:

Eur J Nucl Med Mol Imaging. 2022 September ; 49(11): 3705–3716. doi:10.1007/s00259-022-05814-9.

[^{68}Ga]Ga-FAPI-46 PET for noninvasive detection of pulmonary fibrosis disease activity

Zachary T. Rosenkrans[1], **Christopher F. Massey**[1], **Ksenija Bernau**[2], **Carolina A. Ferreira**[1], **Justin J. Jeffery**[3], **Jefree J. Schulte**[4], **Melissa Moore**[5], **Frank Valla**[5], **Jeanine M. Batterton**[1], **Christopher R. Drake**[5], **Alan B. McMillan**[1], **Nathan Sandbo**[2], **Ali Pirasteh**[1], **Reinier Hernandez**[1,4]

[1]Departments of Medical Physics and Radiology, University of Wisconsin-Madison, Madison, Wisconsin, USA

[2]Department of Medicine, Division of Allergy, Pulmonary and Critical Care Medicine, University of Wisconsin-Madison School of Medicine and Public Health, Madison, Wisconsin

[3]University of Wisconsin Carbone Cancer Center, University of Wisconsin-Madison, Madison, Wisconsin

[4]Department of Pathology and Laboratory Medicine, University of Wisconsin-Madison, Madison, Wisconsin

[5]SOFIE, Dulles, VA, USA.

Abstract

Purpose: The lack of effective molecular biomarkers to monitor idiopathic pulmonary fibrosis (IPF) activity or treatment response remains an unmet clinical need. Herein, we determined the utility of fibroblast activation protein inhibitor for positron emission tomography (FAPI PET) imaging in a mouse model of pulmonary fibrosis.

Methods: Pulmonary fibrosis was induced by intratracheal administration of bleomycin (1 U/kg) while intratracheal saline was administered to control mice. Subgroups from each cohort (n=3–

Corresponding authors: Reinier Hernandez, Ph.D., University of Wisconsin-Madison, Departments of Medical Physics and Radiology, 1111 Highland Ave., Room 7137, Madison, WI 53705, Hernandez6@wisc.edu, Ali Pirasteh, M.D., University of Wisconsin-Madison, Department of Medical Physics and Radiology, 1111 Highland Ave., Room 2423, Madison, WI 53705, Pirasteh@wisc.edu.

Authors' contributions

All authors have contributed to, read, and approved the manuscript. Z.T.R and R.H. conceived the idea and designed the study. Z.T.R., C.F.M., and C.A.F. conducted the imaging experiments. K.B. and N.S. established the pulmonary fibrosis model. J.J.S. analyzed tissue staining. J.M.B. produced Ga-68. M.M., F.V. and C.R.D. prepared the FAPI-46 compound. J.J.J., A.B.M., and A.P. contributed through discussion.

Declarations

Competing Interests

A.P. receives departmental research support from GE Healthcare. A.P. serves as a consultant for TheraCear and Sanofi Genzyme. M.M., F.V., and C.R.D. are all current (F.V.) or former employees (M.M., C.R.D.) at SOFIE. All other authors declare no conflicts of interest.

Ethics approval and consent to participate

All animal studies were conducted under protocols approved by the Institutional Animal Care and Use Committee at the University of Wisconsin-Madison.

Consent for publication

Not applicable

5) underwent dynamic 1 h PET/CT after intravenously injecting FAPI-46 radiolabeled with gallium-68 ([^{68}Ga]Ga-FAPI-46) at 7 d and 14 d following disease induction. Animals were sacrificed following imaging for *ex vivo* gamma counting and histologic correlation. [^{68}Ga]Ga-FAPI-46 uptake was quantified and reported as percent injected activity per cc (%IA/cc) or percent injected activity (%IA). Lung CT density in Hounsfield units (HU) was also correlated with histologic examinations of lung fibrosis.

Results: CT only detected differences in the fibrotic response at 14 d post-bleomycin administration. [^{68}Ga]Ga-FAPI-46 lung uptake was significantly higher in the bleomycin group than in control subjects at 7 d and 14 d. Significantly (P=0.0012) increased [^{68}Ga]Ga-FAPI-46 lung uptake in the bleomycin groups at 14 d (1.01±0.12 %IA/cc) vs. 7 d (0.33±0.09 %IA/cc) at 60 min post-injection of the tracer was observed. These findings were consistent with an increase in both fibrinogenesis and FAP expression as seen in histology.

Conclusion: CT was unable to assess disease activity in a murine model of IPF. Conversely, FAPI PET detected both the presence and activity of lung fibrogenesis, making it a promising tool for assessing early disease activity and evaluating the efficacy of therapeutic interventions in lung fibrosis patients.

Keywords

Fibroblast activation protein; idiopathic; pulmonary fibrosis; positron emission tomography imaging; [^{68}Ga]Ga-FAPI-46

Introduction

Idiopathic pulmonary fibrosis (IPF) is a progressive and irreversible form of fibrotic lung disease affecting approximately 130,000 patients in the United States. IPF carries a poor prognosis, with a five-year survival rate of 20–40% [1–3]. Currently, clinicians utilize a combination of high-resolution computed tomography (CT), pulmonary function test, and biopsy/histology to detect, monitor, and manage IPF. While CT provides excellent anatomic information of the lung structure and disease sequela, it does not provide adequate information regarding functional disease activity. Alternatively, biopsies characterize disease activity but are invasive and carry inherent risks of morbidity and mortality [4, 5]. Overall, diagnostic methods detect morphological and functional lung features that are often non-specific and appear at later stages of the disease, resulting in misdiagnosis, repeated diagnostic testing, and unnecessary or ineffective treatments [6]. Therefore, there is an urgent clinical need for a sensitive noninvasive tool to diagnose early disease activity, monitor therapeutic response, and advance our understanding of the course of this debilitating disease.

Fibroblasts are the principal effector cells driving lung fibrogenesis in IPF [7]. During injury, fibroblast activation results in their migration, proliferation, and remodeling of the lung extracellular matrix, leading to progressive functional deterioration and ultimately lung failure [8]. Fibroblast activation protein-α (FAP) is a serine protease selectively expressed on activated stromal fibroblasts during tissue remodeling and is associated with pulmonary fibrosis [9, 10]. Since FAP expression is relatively low in healthy tissues, this enzyme has

become an attractive molecular target for diverse disease diagnosis and treatment, including epithelial cancers, wound healing, and inflammatory conditions [11–13]. Radiolabeled quinoline-based small molecule fibroblast activation protein inhibitors (FAPI) have been employed as positron emission tomography (PET) radiotracers to noninvasively and quantitatively assess FAP expression [14]. Importantly for preclinical studies, human and murine fibroblast activation protein have an 89% shared sequence identity, and the catalytic domain is conserved.[15, 16] FAPI-derivates have a high affinity for human and murine FAP, although lower affinity for murine FAP than human FAP has been noted.[17] To date, the focus of FAPI PET studies has been cancer detection, given that FAP expression is found in 90% of all epithelial neoplasms [18, 19]. In comparison, the potential of FAPI PET for evaluating non-oncologic disease processes, such as pulmonary fibrosis, remains relatively underexplored.

In this study, we evaluated the potential of FAPI-46 radiolabeled with gallium-68 ([^{68}Ga]Ga-FAPI-46) to noninvasively detect disease activity in a well-established murine model of pulmonary fibrosis [20]. More importantly, since fibroblast activation and FAP expression precedes fibrogenesis [21, 22], we set out to demonstrate that [^{68}Ga]Ga-FAPI-46 is uniquely suited to detect lung fibrosis and monitor disease activity sensitively.

Materials and Methods

Materials

FAPI-46 was provided by SOFIE (Dulles, VA). Anti-FAP antibody was purchase from Abcam (Ab53066). All materials were used as received without further purification.

Radiosynthesis and purification of [^{68}Ga]Ga-FAPI-46 and [^{68}Ga]Ga-DOTA

$^{68}GaCl_3$ was eluted in 0.1 M HCl from a germanium-68/gallium-68 generator (Eckert and Zeigler, Inc.) at the Clinical radiopharmaceutical facility of the University of Wisconsin-Madison and FAPI-46 was radiolabeled as previously described [23–25]. Briefly, a 1 mL $^{68}GaCl_3$ (5–10 mCi) generator fraction was incubated with FAPI-46 (5 nmol/mCi) at 95°C for 15 min in a 0.17 M sodium acetate containing 0.1% sodium ascorbate as previously reported [23]. [^{68}Ga]Ga-FAPI-46 was purified using reverse-phase solid-phase extraction with an Oasis HLB light cartridge (Waters), eluted in neat ethanol, and the eluate was dried under a nitrogen flow and reconstituted in normal saline for injection. Radiochemical yield was determined by radio-instant thin layer chromatography (iTLC) with paper-backed silica plates and 50 mM EDTA as mobile phase. Reverse-phase high-performance liquid chromatography (HPLC) using a C18 column (250 × 3.00 mm, Luna 5μ 100 Å; Phenomenex) and a water (A): acetonitrile (B) multistep gradient (5% B: 0–2 min; 5–65% B: 2–30 min; 65–90% B: 30–35 min; 90–5% B: 35–45 min) was carried out to confirm radiochemical yield and determine radiochemical purity.

[^{68}Ga]Ga-DOTA was prepared using the same radiolabeling procedure for [^{68}Ga]Ga-FAPI-46. Briefly, a 1 mL $^{68}GaCl_3$ (5–10 mCi; 185 – 370 MBq) generator fraction was incubated with DOTA (0.14 nmol/MBq; 5 nmol/mCi) at 95°C for 15 min in a 0.17 M sodium acetate (pH = 5.5) buffer containing 0.1% sodium ascorbate. Radiochemical yields

were confirmed by TLC using MeOH/NH_4OH (1:1) as the mobile phase. [^{68}Ga]Ga-DOTA was diluted for imaging without purification.

Lung Fibrosis Animal Model

The pulmonary fibrosis model and controls were established using 12–16-week-old female and male C57BL/6J mice that were anesthetized with ketamine (100 mg/kg; Zoetis, Inc., Parsippany-Troy Hills, NJ) and xylazine (15 mg/kg; Akorn Pharmaceuticals, Lake Forest, IL). Bleomycin (1 U/kg; Teva Pharmaceuticals, Inc.) dissolved in 50 μL 0.9% normal saline irrigation (Baxter, Madison, WI) was instilled intratracheally into the lung of the animals as previously reported [20, 26]. Control mice were given 0.9% normal saline under the same procedure. Mice were used for imaging studies at 7 d and 14 d following lung injury.

PET/CT imaging and biodistribution

PET/CT scans were acquired using an Inveon small-animal PET/CT scanner (Siemens, Knoxville, TN). CT images were obtained using the following parameters: 80 kVp, 900 μA, and a nominal axial resolution of 105 μm. Volumes of interest (VOI) from CT images were quantified in Hounsfield units (HU). For dynamic PET scanning at 7 d and 14 d following lung injury, mice (n=3) were anesthetized with isoflurane (2%) and the lateral tail vein catheterized. Animals were then placed in the scanner in a prone position and administered approximately 0.8–3.8 MBq (20–100 μCi) [^{68}Ga]Ga-FAPI-46 intravenous bolus, which varied due to the decay of Ga-68 over the study. The specific activity of [^{68}Ga]Ga-FAPI-46 ranged from 0.8–4.8 GBq/μmol over the course of the dynamic scans. One-hour dynamic list-mode PET scans (46 frames) were acquired and reconstructed using an OSEM3D/MAP algorithm. Imaging frames were binned as follows: 12 × 5 s, 6 × 10 s, 6 × 30 s, 10 × 60 s, 6 × 150 s, and 6 × 300 s. Additional mice were injected with approximately 3.8 MBq (100 μCi) of [^{68}Ga]Ga-FAPI-46 for static PET image acquisition at 1 h post-injection (p.i.). Static PET/CT using [^{18}F]FDG purchased from SOFIE (Dulles, VA) was performed in bleomycin and control mice at 60 min p.i. at 6 d and 13 d following PF disease induction. PET/CT at 1 h p.i. using non-specific [^{68}Ga]Ga-DOTA was performed the next day with the same cohort of mice used for [^{18}F]FDG PET/CT. Following the 1 h imaging period in [^{68}Ga]Ga-FAPI-46 PET/CT, the mice were euthanized, and the major organs were collected for *ex vivo* biodistribution. Tissue samples were wet-weighed and counted in an automatic gamma counter (Wizard 2; Perkin Elmer; Waltham, MA) to quantify tracer uptake. Biodistribution data was calculated in percent injected activity (%IA) for the lungs or %IA per gram of tissue (%IA/g) for all other organs of interest.

Image Analysis

Co-registered PET/CT images were displayed as maximum intensity projections at different timepoints post [^{68}Ga]Ga-FAPI-46 injection. Quantitative analysis of the dynamic PET images was carried out in an Inveon Research Workstation (Siemens, Knoxville, TN). Volumes of interest (VOI) of the whole lung were drawn in CT images using an automatic thresholding tool. Whole lung CT VOI were analyzed by comparing the HU in each voxel and determining the relative percentages in various windows (< −600, −500 to −400, −400 to −300, −200 to −100, −100 to 0, and 0 to 100) as previously described [27, 28]. VOI of other organs of interest were drawn manually, and time-activity curves of each VOI were

generated. Quantitative PET imaging data were reported as percent injected activity per cubic centimeter of tissue (%IA/cc).

Histology

Following imaging studies, mice were euthanized, and the lungs were inflated and fixed with 10% formalin overnight and then transferred to 70% ethanol for storage. Lung tissue samples were processed by the UWCCC Translational Research Initiatives in Pathology (TRIP) lab using previously reported methods [20]. Tissues were embedded in paraffin for Masson's trichrome staining and immunohistochemical (IHC) staining of FAP. IHC was performed with an anti-FAP antibody (ab53066; Abcam) at an antibody dilution of 1:50. Human breast cancer tissue available through the TRIP lab was used as a positive control. Omission of the primary antibody was used for the negative control. Stained slides were imaged using Leica Aperio AT2 digital pathology slide scanner. Ashcroft scoring was performed to quantify the degree of fibrosis of Masson Trichrome's stained lung tissue samples as previously described [29].

Statistical analysis

Data and statistical analyses were performed using GraphPad 7.0 (Prism). Quantitative data are expressed as mean ± standard deviation. *P* values were calculated using the Student's t-test. A $p < 0.05$ value was considered statistically significant.

Results

Radiosynthesis of [^{68}Ga]Ga-FAPI-46 and [^{68}Ga]Ga-DOTA

[^{68}Ga]Ga-FAPI-46 radiosynthesis was accomplished in 15 min with quantitative yields (97.8% ± 0.6%) at a molar activity of 7.4 GBq/μmol at the end of chemistry. Radio-HPLC of the radiolabeling reaction showed two measurable radio peaks corresponding to unlabeled ^{68}Ga and [^{68}Ga]Ga-FAPI-46 with retention times of 1.3 min and 8.9 min, respectively. The calculated radiochemical yield based on area integration analysis of the radio-chromatograms was 98.4% (Figure S1). Free ^{68}Ga was undetectable by radio-HPLC in the purified [^{68}Ga]Ga-FAPI-46 product.

CT imaging

CT density of mice administered bleomycin or saline controls was measured at 7 d and 14 d following substance administration (n=5–7; Figure 1, Table S1). The fibrotic response of mice was compared by comparing the relative percentage of CT attenuation values in the voxels of the whole lung VOI. The highest CT attenuation ranges (−200 to +100) correlated with increased density observed with edema or fibrosis. Bleomycin treated mice at 14 d had the highest percentage of voxels (12.4 ± 7.7 %), which was significantly higher compared to saline control mice at 14 d (0.2 ± 0.3 %; P = 0.006) and bleomycin treated mice at 7 d (2.0 ± 1.7 %; P = 0.004). Importantly, CT found no significant differences were found between bleomycin treated mice and control mice at 7 d (2.0 ± 1.7 % vs 0.7 ± 0.5 %, respectively; P = 0.15) nor between control mice at 7 d and 14 d (P = 0.08). Moreover, a significant decrease in the low range HU voxel percentages (−500 to −400 HU) corresponding to lung aeration was found for bleomycin treated mice at 14 d (26.7 ± 8.8 %) compared to

bleomycin treated mice at 7 d (36.9 ± 4.4%; P = 0.018) or control mice at either time point (7 d: 37.9 ± 4.5 %, P = 0.027; 14 d: 41.2 ± 6.3 %, P = 0.0011). Additionally, differences in saline control mice at 7 d and 14 d was not significant (P=0.71). Thus, CT was only able to detect statistically significant differences between mice treated with bleomycin and saline control at 14 d post instillation.

PET/CT imaging with [^{68}Ga]Ga-FAPI-46

We then evaluated the potential of [^{68}Ga]Ga-FAPI-46 to detect fibrotic activity in the lungs using 1 h dynamic PET/CT at 7 d and 14 d following the induction of the bleomycin-injury model (Figure 2, Table S2–S3). In all mice, both imaging timepoints showed rapid uptake of [^{68}Ga]Ga-FAPI-46 in the lungs, followed by slow tracer elimination. Similar uptake and clearance of [^{68}Ga]Ga-FAPI-46 was observed in the blood and liver (Figure S2–S3). Peak uptake of [^{68}Ga]Ga-FAPI-46 in the kidneys of bleomycin mice was slightly delayed with slower clearance compared to control mice, which may be due to off target effects of renally eliminated bleomycin [30]. Using a two-phase exponential decay fit of the [^{68}Ga]Ga-FAPI-46 time-activity curve of the blood pool, we estimated comparable slow and fast circulation half-lives in bleomycin (slow: 6.1 min, fast: 0.23 min) and control (slow: 5.8 min, fast: 0.23 min) mice (Table S4), at 7 d after bleomycin instillation. A similar analysis of [^{68}Ga]Ga-FAPI-46 in the blood pool at 14 d after bleomycin injury found slow and fast half-lives of bleomycin (slow: 3.2 min, fast: 0.15 min) and control (slow: 6.1 min, fast: 0.58 min) mice (Table S5). Kidneys had the highest and most prolonged uptake among the analyzed tissues, evidencing renal elimination as the primary route of excretion for [^{68}Ga]Ga-FAPI-46. All other analyzed tissues displayed marginal [^{68}Ga]Ga-FAPI-46 uptake below 4 %IA/cc.

Significantly higher [^{68}Ga]Ga-FAPI-46 uptake in the lungs of diseased mice compared to healthy mice was found as early as 15 min p.i. of the radiotracer for imaging studies at 7 d and 14 d following lung injury. Based on these findings, we compared tracer uptake at 30 min and 60 min p.i. to evaluate the ability of [^{68}Ga]Ga-FAPI-46 to detect changes in disease activity in the lungs between 7 d and 14 d (Figure 3). Both 30 min and 60 min p.i. [^{68}Ga]Ga-FAPI-46 PET/CT static images identified fibroblast activation in the lungs of mice treated with bleomycin compared to controls for both post-injury timepoints. VOI analysis of the whole lung at 7 d post bleomycin administration revealed a 1.8-fold higher uptake in bleomycin (0.76±0.13 %IA/cc) vs. control (0.43±0.04 %IA/cc mice; p=0.014) at 30 min p.i., and 2.6-fold higher uptake in bleomycin mice (0.33±0.09 %IA/cc) vs. control mice (0.13±0.06; p=0.007) at 60 min p.i. These differences increased further to 2.2-fold higher uptake at 30 min p.i. (1.47±0.15 %IA/cc vs. 0.66±0.15 %IA/cc; p=0.0025) and 4-fold higher uptake at 60 min p.i. (1.01±0.12 %IA/cc vs. 0.25±0.15 %IA/cc; p=0.0003) in bleomycin vs. controls, at 14 d post-bleomycin instillation. Importantly, uptake in the lungs significantly increased at 30 min p.i. from 0.76±0.13 %IA/cc to 1.47±0.15 %IA/cc (p=0.0035) as injury progressed from 7 d to 14 d after bleomycin administration, indicating increased fibroblast activity and fibrogenesis. Similarly, 60 min p.i. [^{68}Ga]Ga-FAPI-46 uptake in the fibrotic lung also increased significantly from 0.33±0.09 %IA/cc at 7 d to 1.01±0.12 %IA/cc (p=0.0012) at 14 d. In comparison, VOI quantification of whole lung uptake in control mice at 7 d vs. 14 d was not significant at 30 min p.i. (0.43 ± 0.04 %IA/cc vs 0.66 ± 0.15 %IA/cc;

p = 0.06) nor at 60 min p.i. (0.13 ± 0.06 %IA/cc vs 0.25 ± 0.15 %IA/cc; p = 0.12). *Ex vivo* biodistribution studies following the imaging studies at 7 d and 14 d, corroborated [^{68}Ga]Ga-FAPI-46 quantitative PET imaging data at 60 min p.i. and provided additional information on normal tissue distribution of the radiotracer (Figure 4, Figure S4–S5, Table S6–S7). Consistently, significantly higher lung uptake in bleomycin mice was observed compared to control mice at 7 d (bleomycin: 0.21±0.03 %IA, control: 0.05±0.02 %IA, p=0.0013). At 14 d after model induction, overall lung uptake for bleomycin mice compared to control was also significantly higher (bleomycin: 0.59±0.39 %IA, control: 0.08±0.06 %IA, p=0.024).

PET/CT imaging with [^{18}F]FDG and [^{68}Ga]Ga-DOTA

Other biological phenomena such as blood flow, edema, or inflammation may lead to non-specific lung uptake of [^{68}Ga]Ga-FAPI-46 in bleomycin mice. To determine the contribution of these factors and confirm the specificity of [^{68}Ga]Ga-FAPI-46, control PET/CT studies were performed using [^{18}F]FDG. Previous studies have found that [^{18}F]FDG, a glucose metabolism radiotracer, can visualize the inflammatory and fibrotic processes during PF [31]. As such, we compared [^{18}F]FDG PET to FAPI PET by acquiring images at 60 min p.i. at 6 d and 13 d following PF disease induction (Figure 5). Notably, VOI analysis found 1.7-fold higher uptake of [^{18}F]FDG in the lungs of bleomycin mice (4.57±0.95 %IA/cc) compared to control mice (2.67±0.67 %IA/cc) at 6 d following bleomycin administration. However, the lung uptake in bleomycin mice (3.88±0.95 %IA/cc) slightly decreased at 13 d following disease induction to 1.4-fold higher than control mice (2.75±0.25 %IA/cc). Moreover, high background of [^{18}F]FDG in the heart and central nervous system may introduce signal spillover effects that complicate VOI analysis of lungs in preclinical studies.

Additional control imaging studies in bleomycin and control mice were performed using [^{68}Ga]Ga-DOTA, the chelator portion of FAPI-46 with no targeting properties (Figure S5). PET/CT using [^{68}Ga]Ga-DOTA was performed at 60 min p.i. at 7 d and 14 d following bleomycin or saline administration, and VOI analysis found negligible lung uptake in all groups and timepoints. No significant differences between mice given bleomycin or control was found.

Histology and immunohistochemistry

To correlate [^{68}Ga]Ga-FAPI-46 lung uptake with *in situ* FAP expression and fibrosis, the whole lungs of imaged mice were perfused and harvested for histopathological characterization of fibrosis and FAP expression (Figure 6a, Figure S6–S7). Masson's trichrome staining showed marked collagen deposition in the lungs of diseased mice, which progressively worsened from 7 d to 14 d after lung injury. Minimal fibrosis was observed in mice intratracheally treated with saline. Ashcroft histopathological scoring of lung tissue found a significant fibrotic response in mice treated with bleomycin compared to saline controls at both 7 d (control = 0.04 ± 0.08, bleomycin = 0.45 ± 0.09; p = 0.004) and 14 d (control = 0.03 ± 0.03, bleomycin = 1.14 ± 0.53; p = 0.022) post instillation (Figure 6b). While not significantly different (p=0.088), Ashcroft score of mice treated with bleomycin increased from 7 d to 14 d post instillation, demonstrating increased fibrosis disease activity. Importantly, Ashcroft histopathological scoring correlated with FAPI PET data.

Similarly, immunohistochemical analysis of FAP expression revealed notable FAP staining in the lungs of mice administered bleomycin. Both the intensity and density of FAP staining were markedly higher at 14 d following bleomycin-instillation than at 7 d or in control mice; the latter displayed negligible FAP expression. It is important to note that FAP IHC staining had significant background staining that could be optimized in future studies. However, fibrotic lesions stained positive for FAP expression above background and correlated with Trichrome staining. Overall, increased [^{68}Ga]Ga-FAPI-46 uptake correlated qualitatively with higher FAP expression and the degree of lung fibrosis.

Discussion

IPF is a chronic and progressive lung disease without a known cause. Patients often present with exertional dyspnea that may occur in conjunction with a dry cough and have a poor quality of life [32]. A timely IPF diagnosis is among the most difficult challenges patients and clinicians face because of the non-specific symptoms of early disease, which overlap with those of other common pulmonary diseases or aging [6]. Currently, clinical diagnosis of IPF relies on CT imaging and invasive lung tissue biopsy in selected patients. Lung biopsies carry considerable risk in elderly patients, the most common IPF patient demographic [33]. CT features can be non-diagnostic, do not provide information of disease activity, or provide biological information on the underlying pathology. Consequently, patients can be symptomatic for more than 5 years before an IPF diagnosis is made, making early therapeutic interventions unattainable [34]. There is an urgent need for novel noninvasive diagnostic methods and prognostic methods that rely on biomarkers relevant to IPF in the clinic.

IPF is a disorder of aberrant epithelial injury and dysregulated tissue repair [35]. Activated fibroblasts have been identified as the key effector cells that mediate the extracellular matrix remodeling in pulmonary fibrosis [36]. Positive feedback from fibroblasts and an aberrant extracellular matrix lead to progressive fibrotic scarring, functional decline, and ultimately lung failure [37]. FAP, which is not expressed in healthy adult lungs, is selectively expressed in activated fibroblasts during the pathogenic tissue remodeling that occurs during chronic inflammation, wound healing, or fibrosis [9, 38–40]. Previous studies have shown that FAP expression increases in murine models of pulmonary fibrosis and correlates with severity of lung injury [41]. However, conflicting accounts on the role of FAP in lung fibrogenesis exist. While Fan and colleagues reported that FAP protects lungs by degrading matrix and reducing collagen content, other studies found that a FAP inhibitor had anti-fibrotic effects and slowed disease progression [42, 43]. Although FAP was found in the fibrotic foci of adult human IPF patients, the significance of FAP expression during the different stages of the disease remains unclear [9]. Recently, Röhrich et al. evaluated FAPI-PET in human subjects with fibrotic interstitial lung disease (fILD) and lung cancer [44]. FAPI-PET uptake was markedly increased in fibrotic lesions, which was also detected histologically. Another recent study by Bergmann et al. found that FAPI-PET uptake increased in the fibrotic lung regions of patients with systemic sclerosis-associated interstitial lung disease [45]. Moreover, fibrotic activity and disease activity were correlated to fibroblast activation. These promising results of FAPI-PET in interstitial lung diseases subtypes highlight the need for

further investigation into the role FAP in IPF pathogenesis and progression, as well as its role as a potential biomarker for early disease activity.

We investigated whether [^{68}Ga]Ga-FAPI-46 PET/CT can detect *in vivo* FAP expression and monitor the disease severity noninvasively in a mouse model of pulmonary fibrosis. Our results showed that [^{68}Ga]Ga-FAPI-46 PET was able to detect lung injury in a bleomycin pulmonary fibrosis model and detect increased fibrogenesis in a model of pulmonary fibrosis. Dynamic PET revealed statistically higher lung uptake of [^{68}Ga]Ga-FAPI-46 in bleomycin treated mice compared with saline controls even at 7 d following injury when relatively low levels of fibrosis (collagen deposition) are observed. Importantly, we detected an increase in lung uptake of [^{68}Ga]Ga-FAPI-46 in diseased animals from 7 d to 14 d that was consistent with the heightened FAP expression and extracellular matrix deposition observed by histology in the pulmonary fibrosis model at 14 d [46]. Moreover, Ashcroft scoring of lung tissue similarly reflected [^{68}Ga]Ga-FAPI-46 lung uptake observed in VOI quantification and *ex vivo* biodistribution analysis. It should be noted that the imaging study at 7 d post-bleomycin occurred during the acute inflammatory phase of the bleomycin animal model that may confound [^{68}Ga]Ga-FAPI-46 PET imaging results by increasing non-specific radiotracer uptake [47–49]. However, the imaging study at 14 d post-bleomycin was performed during the peak pro-fibrotic phase, in which inflammation has largely subsided [49, 50]. Importantly, when [^{18}F]FDG was employed for monitoring PF disease activity, the lung uptake was highest during the inflammatory phase of the model (6 d post induction) and slightly decreased, although not significantly, during the profibrotic phase of the model (13 d post induction), indicating reduced lung inflammation at the latter timepoint. Moreover, PET quantification of [^{18}F]FDG uptake was complicated by high metabolic uptake in the heart and central nervous system. Other control PET studies using non-targeted [^{68}Ga]Ga-DOTA found negligible lung uptake in mice treated with saline or bleomycin. Taken together, these studies indicate that [^{68}Ga]Ga-FAPI-46 specifically targets FAP and that non-specifc uptake or inflammation had little contribution to the increased [^{68}Ga]Ga-FAPI-46 lung uptake observed in diseased lungs at 14 d following bleomycin instillation. In future studies, we will determine the sensitivity of [^{68}Ga]Ga-FAPI-46 PET to detect disease activity longitudinally in slower-progressing, more specific, models of pulmonary fibrosis that better resemble the course of the human disease [51].

Notably, CT only detected differences between bleomycin treated mice and control mice at 14 post blemycin instillation. Moreover, CT assessment at early timepoints is compliated by the presence of CT-opaque pulmonary edema during the inflammatory phase of the bleomycin model. The radiological confounding factors together with the fact that CT can only detect architectural changes on lung tissue, are the reason why CT provides limited information about disease activity and fails to predict the evolution or treatment response in IPF patients [52]. Therefore, noninvasive imaging modalities such as [^{68}Ga]Ga-FAPI-46 PET providing not only spatial but also functional information about disease activity pose tremendous benefits for early diagnosis of IPF.

Other PET and MR molecular agents have been tested for noninvasively detecting pulmonary fibrosis based on different aspects of IPF pathobiology, including enhance glucose metabolism, or the expression of cathepsin proteases, collagen type I, integrin $\alpha_v\beta_6$,

chemokine receptor 2, and others [52–59]. Of these, ^{18}F-fluorodeoxyglucose ([^{18}F]-FDG) PET/CT has been utilized the most in clinical studies and has been able to detect severe IPF. However, [^{18}F]-FDG PET/CT visualizes elevated glucose metabolism that occurs in cells during inflammatory processes and is non-specific to any IPF-specific molecular targets [60]. Previous studies using [^{18}F]-FDG uptake peaked at 14 d post-bleomycin administration and was significantly higher compared to saline controls at the late fibrotic phase of the model (24 d post-bleomycin administration), which was attributed to increased glucose of proliferating fibroblasts or myfibroblasts producing collagen but lacks specificity [41]. Compared to these radiotracers, [^{68}Ga]Ga-FAPI-46 PET has several advantages as a specific biomarker for the detection of IPF. Since fibroblasts drive fibrogenesis [61], detecting activated fibroblasts using FAPI PET may enable real-time assessment of disease activity in addition to prognostic information, which current imaging modalities do not provide. Furthermore, FAPI PET could be employed to assess individual therapeutic responses to pharmaceutical agents targeting fibroblast activation. Finally, since activated fibroblasts are the initiators of tissue fibrosis, FAPI PET could more sensitively detect pro-fibrotic disease earlier than other agents during the molecular events leading to IPF. Thus, patients with IPF could be inequivocally diagnosed earlier resulting in more timely interventions and potentially better treatment outcomes. Finally, the breadth of applications for FAPI PET agents is highlighted by their use in various preclinical and clinical investigations for detecting pathologyaclly activated fibroblast, which have established the safety and sensitivity of these tracers in non-oncological diseases, as well as different cancer types.

Conclusion

The ability of FAPI PET to successfully detect both presence and disease activity in a murine model of pulmonary fibrosis makes it a promising tool for clinical evaluation of lung fibrosis in humans. By annotating the fibroblast activation protein expression, noninvasive PET with [^{68}Ga]Ga-FAPI-46 has the potential to detect the early onset of fibrotic injury at earlier stages of the disease where current diagnostic tools such as high resolution-lung CT or spirometry provide inadequate diagnostic sensitivity. Our results warrant further exploration of [^{68}Ga]Ga-FAPI-46 PET for the detection of pulmonary fibrosis and other fibrotic diseases in humans.

Supplementary Material

Refer to Web version on PubMed Central for supplementary material.

Acknowledgements

The authors wish to acknowledge the Small Animal Imaging and Radiotherapy (SAIRF) facility at UW-Madison maintaining facilities for acquiring PET/CT, including support through the Cancer Center Support Grant NCI P30CA014520. The author(s) thank the University of Wisconsin Translational Research Initiatives in Pathology laboratory (TRIP), supported by the UW Department of Pathology and Laboratory Medicine, UWCCC (P30 CA014520) and the Office of The Director- NIH (S10 OD023526) for use of its facilities and services."

Funding

This work was supported by the University of Wisconsin-Madison, the National Institutes of Health (R01HL146402), and Department of Defense (Early Investigator Award, W81XWH1910285). Research reported in

this publication was supported by the National Cancer Institute of the National Institutes of Health under Award Number T32CA009206. The content is solely the responsibility of the authors and does not necessarily represent the official views of the National Institutes of Health.

Availability of data and materials

The datasets used and/or analysed during the current study are available from the corresponding author on reasonable request.

References

1. Rafii R, Juarez MM, Albertson TE, Chan AL. A review of current and novel therapies for idiopathic pulmonary fibrosis. Journal of Thoracic Disease. 2013;5:48–73. [PubMed: 23372951]
2. Martinez FJ, Collard HR, Pardo A, Raghu G, Richeldi L, Selman M, et al. Idiopathic pulmonary fibrosis. Nature Reviews Disease Primers. 2017;3:17074. doi:10.1038/nrdp.2017.74.
3. Hutchinson J, Fogarty A, Hubbard R, McKeever T. Global incidence and mortality of idiopathic pulmonary fibrosis: a systematic review. European Respiratory Journal. 2015;46:795–806. doi:10.1183/09031936.00185114. [PubMed: 25976683]
4. Lorenz J, Blum M. Complications of percutaneous chest biopsy. Semin Intervent Radiol. 2006;23:188–93. doi:10.1055/s-2006-941449. [PubMed: 21326762]
5. Hutchinson JP, Fogarty AW, McKeever TM, Hubbard RB. In-Hospital Mortality after Surgical Lung Biopsy for Interstitial Lung Disease in the United States. 2000 to 2011. Am J Respir Crit Care Med. 2016;193:1161–7. doi:10.1164/rccm.201508-1632OC. [PubMed: 26646481]
6. Spagnolo P, Ryerson CJ, Putman R, Oldham J, Salisbury M, Sverzellati N, et al. Early diagnosis of fibrotic interstitial lung disease: challenges and opportunities. Lancet Respir Med. 2021. doi:10.1016/S2213-2600(21)00017-5.
7. Wolters PJ, Collard HR, Jones KD. Pathogenesis of idiopathic pulmonary fibrosis. Annual review of pathology. 2014;9:157–79. doi:10.1146/annurev-pathol-012513-104706.
8. Hardie WD, Glasser SW, Hagood JS. Emerging Concepts in the Pathogenesis of Lung Fibrosis. The American Journal of Pathology. 2009;175:3–16. doi:10.2353/ajpath.2009.081170. [PubMed: 19497999]
9. Acharya PS, Zukas A, Chandan V, Katzenstein A-LA, Puré E. Fibroblast activation protein: a serine protease expressed at the remodeling interface in idiopathic pulmonary fibrosis. Human Pathology. 2006;37:352–60. doi:10.1016/j.humpath.2005.11.020. [PubMed: 16613331]
10. Fitzgerald AA, Weiner LM. The role of fibroblast activation protein in health and malignancy. Cancer and Metastasis Reviews. 2020;39:783–803. doi:10.1007/s10555-020-09909-3. [PubMed: 32601975]
11. Altmann A, Haberkorn U, Siveke J. The Latest Developments in Imaging of Fibroblast Activation Protein. Journal of Nuclear Medicine. 2021;62:160–7. doi:10.2967/jnumed.120.244806. [PubMed: 33127618]
12. Kratochwil C, Flechsig P, Lindner T, Abderrahim L, Altmann A, Mier W, et al. 68Ga-FAPI PET/CT: Tracer Uptake in 28 Different Kinds of Cancer. Journal of Nuclear Medicine. 2019;60:801–5. doi:10.2967/jnumed.119.227967. [PubMed: 30954939]
13. Watabe T, Liu Y, Kaneda-Nakashima K, Shirakami Y, Lindner T, Ooe K, et al. Theranostics Targeting Fibroblast Activation Protein in the Tumor Stroma: 64Cu- and 225Ac-Labeled FAPI-04 in Pancreatic Cancer Xenograft Mouse Models. Journal of Nuclear Medicine. 2020;61:563–9. doi:10.2967/jnumed.119.233122. [PubMed: 31586001]
14. Syed M, Flechsig P, Liermann J, Windisch P, Staudinger F, Akbaba S, et al. Fibroblast activation protein inhibitor (FAPI) PET for diagnostics and advanced targeted radiotherapy in head and neck cancers. European Journal of Nuclear Medicine and Molecular Imaging. 2020;47:2836–45. doi:10.1007/s00259-020-04859-y. [PubMed: 32447444]
15. Niedermeyer J, Scanlan MJ, Garin-Chesa P, Daiber C, Fiebig HH, Old LJ, et al. Mouse fibroblast activation protein: Molecular cloning, alternative splicing and expression in the

reactive stroma of epithelial cancers. International Journal of Cancer. 1997;71:383–9. doi:10.1002/(SICI)1097-0215(19970502)71:3<383::AID-IJC14>3.0.CO;2-H. [PubMed: 9139873]

16. Goldstein LA, Ghersi G, Piñeiro-Sánchez ML, Monica S, Yeh Y, Flessate D, et al. Molecular cloning of seprase: a serine integral membrane protease from human melanoma. Biochimica et Biophysica Acta (BBA) - Molecular Basis of Disease. 1997;1361:11–9. doi:10.1016/S0925-4439(97)00032-X. [PubMed: 9247085]
17. Millul J, Bassi G, Mock J, Elsayed A, Pellegrino C, Zana A, et al. An ultra-high-affinity small organic ligand of fibroblast activation protein for tumor-targeting applications. Proceedings of the National Academy of Sciences. 2021;118:e2101852118. doi:doi:10.1073/pnas.2101852118.
18. Sollini M, Kirienko M, Gelardi F, Fiz F, Gozzi N, Chiti A. State-of-the-art of FAPI-PET imaging: a systematic review and meta-analysis. European Journal of Nuclear Medicine and Molecular Imaging. 2021. doi:10.1007/s00259-021-05475-0.
19. Calais J FAP: The Next Billion Dollar Nuclear Theranostics Target? Journal of Nuclear Medicine. 2020;61:163–5. doi:10.2967/jnumed.119.241232. [PubMed: 31924719]
20. Bernau K, Leet JP, Bruhn EM, Tubbs AJ, Zhu T, Sandbo N. Expression of serum response factor in the lung mesenchyme is essential for development of pulmonary fibrosis. American Journal of Physiology-Lung Cellular and Molecular Physiology. 2021;321:L174–L88. doi:10.1152/ajplung.00323.2020. [PubMed: 33978489]
21. Phan THG, Paliogiannis P, Nasrallah GK, Giordo R, Eid AH, Fois AG, et al. Emerging cellular and molecular determinants of idiopathic pulmonary fibrosis. Cell Mol Life Sci. 2021;78:2031–57. doi:10.1007/s00018-020-03693-7. [PubMed: 33201251]
22. Richeldi L, Collard HR, Jones MG. Idiopathic pulmonary fibrosis. The Lancet. 2017;389:1941–52. doi:10.1016/S0140-6736(17)30866-8.
23. Meyer C, Dahlbom M, Lindner T, Vauclin S, Mona C, Slavik R, et al. Radiation Dosimetry and Biodistribution of 68Ga-FAPI-46 PET Imaging in Cancer Patients. Journal of Nuclear Medicine. 2020;61:1171–7. doi:10.2967/jnumed.119.236786. [PubMed: 31836685]
24. Loktev A, Lindner T, Burger E-M, Altmann A, Giesel F, Kratochwil C, et al. Development of Fibroblast Activation Protein–Targeted Radiotracers with Improved Tumor Retention. Journal of Nuclear Medicine. 2019;60:1421–9. doi:10.2967/jnumed.118.224469. [PubMed: 30850501]
25. Röhrich M, Naumann P, Giesel FL, Choyke P, Staudinger F, Wefers A, et al. Impact of 68Ga-FAPI-PET/CT imaging on the therapeutic management of primary and recurrent pancreatic ductal adenocarcinomas. Journal of Nuclear Medicine. 2020:jnumed.120.253062. doi:10.2967/jnumed.120.253062.
26. Bernau K, Ngam C, Torr EE, Acton B, Kach J, Dulin NO, et al. Megakaryoblastic leukemia-1 is required for the development of bleomycin-induced pulmonary fibrosis. Respiratory Research. 2015;16:45. doi:10.1186/s12931-015-0206-6. [PubMed: 25885656]
27. Bernau K, Skibba M, Leet JP, Furey S, Gehl C, Li Y, et al. Selective Inhibition of Bromodomain-Containing Protein 4 Reduces Myofibroblast Transdifferentiation and Pulmonary Fibrosis. Frontiers in Molecular Medicine. 2022;2. doi:10.3389/fmmed.2022.842558.
28. Scotton CJ, Hayes B, Alexander R, Datta A, Forty EJ, Mercer PF, et al. Ex vivo micro-computed tomography analysis of bleomycin-induced lung fibrosis for preclinical drug evaluation. European Respiratory Journal. 2013;42:1633. doi:10.1183/09031936.00182412. [PubMed: 23520313]
29. Ashcroft T, Simpson JM, Timbrell V. Simple method of estimating severity of pulmonary fibrosis on a numerical scale. J Clin Pathol. 1988;41:467–70. doi:10.1136/jcp.41.4.467. [PubMed: 3366935]
30. Dorr RT. Bleomycin pharmacology: mechanism of action and resistance, and clinical pharmacokinetics. Semin Oncol. 1992;19:3–8.
31. Bondue B, Sherer F, Van Simaeys G, Doumont G, Egrise D, Yakoub Y, et al. PET/CT with 18F-FDG– and 18F-FBEM–Labeled Leukocytes for Metabolic Activity and Leukocyte Recruitment Monitoring in a Mouse Model of Pulmonary Fibrosis. Journal of Nuclear Medicine. 2015;56:127–32. doi:10.2967/jnumed.114.147421. [PubMed: 25537989]
32. Lederer DJ, Martinez FJ. Idiopathic Pulmonary Fibrosis. New England Journal of Medicine. 2018;378:1811–23. doi:10.1056/NEJMra1705751. [PubMed: 29742380]

33. Vaszar LT, Larsen BT, Swanson KL, Ryu JH, Tazelaar HD. Diagnostic utility of surgical lung biopsies in elderly patients with indeterminate interstitial lung disease. Respirology. 2018;23:507–11. doi:10.1111/resp.13223. [PubMed: 29178216]
34. Hewson T, McKeever TM, Gibson JE, Navaratnam V, Hubbard RB, Hutchinson JP. Timing of onset of symptoms in people with idiopathic pulmonary fibrosis. Thorax. 2018;73:683–5. doi:10.1136/thoraxjnl-2017-210177.
35. Moss BJ, Ryter SW, Rosas IO. Pathogenic Mechanisms Underlying Idiopathic Pulmonary Fibrosis. Annual review of pathology. 2021. doi:10.1146/annurev-pathol-042320-030240.
36. Hung C, Linn G, Chow Y-H, Kobayashi A, Mittelsteadt K, Altemeier WA, et al. Role of Lung Pericytes and Resident Fibroblasts in the Pathogenesis of Pulmonary Fibrosis. American journal of respiratory and critical care medicine. 2013;188:820–30. doi:10.1164/rccm.201212-2297OC. [PubMed: 23924232]
37. Parker MW, Rossi D, Peterson M, Smith K, Sikström K, White ES, et al. Fibrotic extracellular matrix activates a profibrotic positive feedback loop. The Journal of Clinical Investigation. 2014;124:1622–35. doi:10.1172/JCI71386. [PubMed: 24590289]
38. Liao Y, Ni Y, He R, Liu W, Du J. Clinical implications of fibroblast activation protein-α in non-small cell lung cancer after curative resection: a new predictor for prognosis. Journal of Cancer Research and Clinical Oncology. 2013;139:1523–8. doi:10.1007/s00432-013-1471-8. [PubMed: 23835897]
39. Varasteh Z, Mohanta S, Robu S, Braeuer M, Li Y, Omidvari N, et al. Molecular Imaging of Fibroblast Activity After Myocardial Infarction Using a 68Ga-Labeled Fibroblast Activation Protein Inhibitor, FAPI-04. Journal of Nuclear Medicine. 2019;60:1743–9. doi:10.2967/jnumed.119.226993. [PubMed: 31405922]
40. Jacob M, Chang L, Puré E. Fibroblast activation protein in remodeling tissues. Current molecular medicine. 2012;12:1220–43. doi:10.2174/156652412803833607. [PubMed: 22834826]
41. Wenlong L, Leilei Y, Wei F, Yi C, Jing T, Lanzhi M, et al. Luciferase expression is driven by the promoter of fibroblast activation protein-α in murine pulmonary fibrosis. Biotechnology Letters. 2015;37:1757–63. doi:10.1007/s10529-015-1855-8. [PubMed: 25994578]
42. Fan M-H, Zhu Q, Li H-H, Ra H-J, Majumdar S, Gulick DL, et al. Fibroblast Activation Protein (FAP) Accelerates Collagen Degradation and Clearance from Lungs in Mice*. Journal of Biological Chemistry. 2016;291:8070–89. doi:10.1074/jbc.M115.701433. [PubMed: 26663085]
43. Egger C, Cannet C, Gérard C, Suply T, Ksiazek I, Jarman E, et al. Effects of the fibroblast activation protein inhibitor, PT100, in a murine model of pulmonary fibrosis. European Journal of Pharmacology. 2017;809:64–72. doi:10.1016/j.ejphar.2017.05.022. [PubMed: 28506908]
44. Röhrich M, Leitz D, Glatting FM, Wefers AK, Weinheimer O, Flechsig P, et al. Fibroblast Activation Protein specific PET/CT imaging in fibrotic interstitial lung diseases and lung cancer: a translational exploratory study. Journal of Nuclear Medicine. 2021:jnumed.121.261925. doi:10.2967/jnumed.121.261925.
45. Bergmann C, Distler JHW, Treutlein C, Tascilar K, Müller A-T, Atzinger A, et al. 68Ga-FAPI-04 PET-CT for molecular assessment of fibroblast activation and risk evaluation in systemic sclerosis-associated interstitial lung disease: a single-centre, pilot study. The Lancet Rheumatology. 2021;3:e185–e94. doi:10.1016/S2665-9913(20)30421-5.
46. Izbicki G, Segel MJ, Christensen TG, Conner MW, Breuer R. Time course of bleomycin-induced lung fibrosis. International Journal of Experimental Pathology. 2002;83:111–9. doi:10.1046/j.1365-2613.2002.00220.x. [PubMed: 12383190]
47. Williamson JD, Sadofsky LR, Hart SP. The pathogenesis of bleomycin-induced lung injury in animals and its applicability to human idiopathic pulmonary fibrosis. Experimental Lung Research. 2015;41:57–73. doi:10.3109/01902148.2014.979516. [PubMed: 25514507]
48. Bleeker-Rovers CP, Boerman OC, Rennen HJ, Corstens FH, Oyen WJ. Radiolabeled compounds in diagnosis of infectious and inflammatory disease. Curr Pharm Des. 2004;10:2935–50. doi:10.2174/1381612043383539. [PubMed: 15379660]
49. Chaudhary NI, Schnapp A, Park JE. Pharmacologic differentiation of inflammation and fibrosis in the rat bleomycin model. American journal of respiratory and critical care medicine. 2006;173:769–76. doi:10.1164/rccm.200505-717OC. [PubMed: 16415276]

50. Moeller A, Ask K, Warburton D, Gauldie J, Kolb M. The bleomycin animal model: A useful tool to investigate treatment options for idiopathic pulmonary fibrosis? The International Journal of Biochemistry & Cell Biology. 2008;40:362–82. doi:10.1016/j.biocel.2007.08.011. [PubMed: 17936056]
51. Shea BS, Brooks SF, Fontaine BA, Chun J, Luster AD, Tager AM. Prolonged exposure to sphingosine 1-phosphate receptor-1 agonists exacerbates vascular leak, fibrosis, and mortality after lung injury. American journal of respiratory cell and molecular biology. 2010;43:662–73. doi:10.1165/rcmb.2009-0345OC. [PubMed: 20081052]
52. Désogère P, Tapias LF, Hariri LP, Rotile NJ, Rietz TA, Probst CK, et al. Type I collagen–targeted PET probe for pulmonary fibrosis detection and staging in preclinical models. Science Translational Medicine. 2017;9:eaaf4696. doi:10.1126/scitranslmed.aaf4696. [PubMed: 28381537]
53. Meissner HH, Soo Hoo GW, Khonsary SA, Mandelkern M, Brown CV, Santiago SM. Idiopathic Pulmonary Fibrosis: Evaluation with Positron Emission Tomography. Respiration. 2006;73:197–202. doi:10.1159/000088062. [PubMed: 16141712]
54. Withana NP, Ma X, McGuire HM, Verdoes M, van der Linden WA, Ofori LO, et al. Non-invasive Imaging of Idiopathic Pulmonary Fibrosis Using Cathepsin Protease Probes. Sci Rep. 2016;6:19755. doi:10.1038/srep19755. [PubMed: 26797565]
55. Kimura RH, Wang L, Shen B, Huo L, Tummers W, Filipp FV, et al. Evaluation of integrin αvβ6 cystine knot PET tracers to detect cancer and idiopathic pulmonary fibrosis. Nature Communications. 2019;10:4673. doi:10.1038/s41467-019-11863-w.
56. Brody SL, Gunsten SP, Luehmann HP, Sultan DH, Hoelscher M, Heo GS, et al. Chemokine Receptor 2–targeted Molecular Imaging in Pulmonary Fibrosis. American journal of respiratory and critical care medicine. 2021;203:78–89. doi:10.1164/rccm.202004-1132OC. [PubMed: 32673071]
57. Désogère P, Tapias LF, Rietz TA, Rotile N, Blasi F, Day H, et al. Optimization of a Collagen-Targeted PET Probe for Molecular Imaging of Pulmonary Fibrosis. J Nucl Med. 2017;58:1991–6. doi:10.2967/jnumed.117.193532. [PubMed: 28611243]
58. Wahsner J, Désogère P, Abston E, Graham-O'Regan KA, Wang J, Rotile NJ, et al. (68)Ga-NODAGA-Indole: An Allysine-Reactive Positron Emission Tomography Probe for Molecular Imaging of Pulmonary Fibrogenesis. J Am Chem Soc. 2019;141:5593–6. doi:10.1021/jacs.8b12342. [PubMed: 30908032]
59. Akam EA, Abston E, Rotile NJ, Slattery HR, Zhou IY, Lanuti M, et al. Improving the reactivity of hydrazine-bearing MRI probes for in vivo imaging of lung fibrogenesis. Chem Sci. 2020;11:224–31. doi:10.1039/c9sc04821a. [PubMed: 32728411]
60. Win T, Screaton NJ, Porter JC, Ganeshan B, Maher TM, Fraioli F, et al. Pulmonary 18F-FDG uptake helps refine current risk stratification in idiopathic pulmonary fibrosis (IPF). European Journal of Nuclear Medicine and Molecular Imaging. 2018;45:806–15. doi:10.1007/s00259-017-3917-8. [PubMed: 29335764]
61. Wynn TA, Ramalingam TR. Mechanisms of fibrosis: therapeutic translation for fibrotic disease. Nature Medicine. 2012;18:1028–40. doi:10.1038/nm.2807.

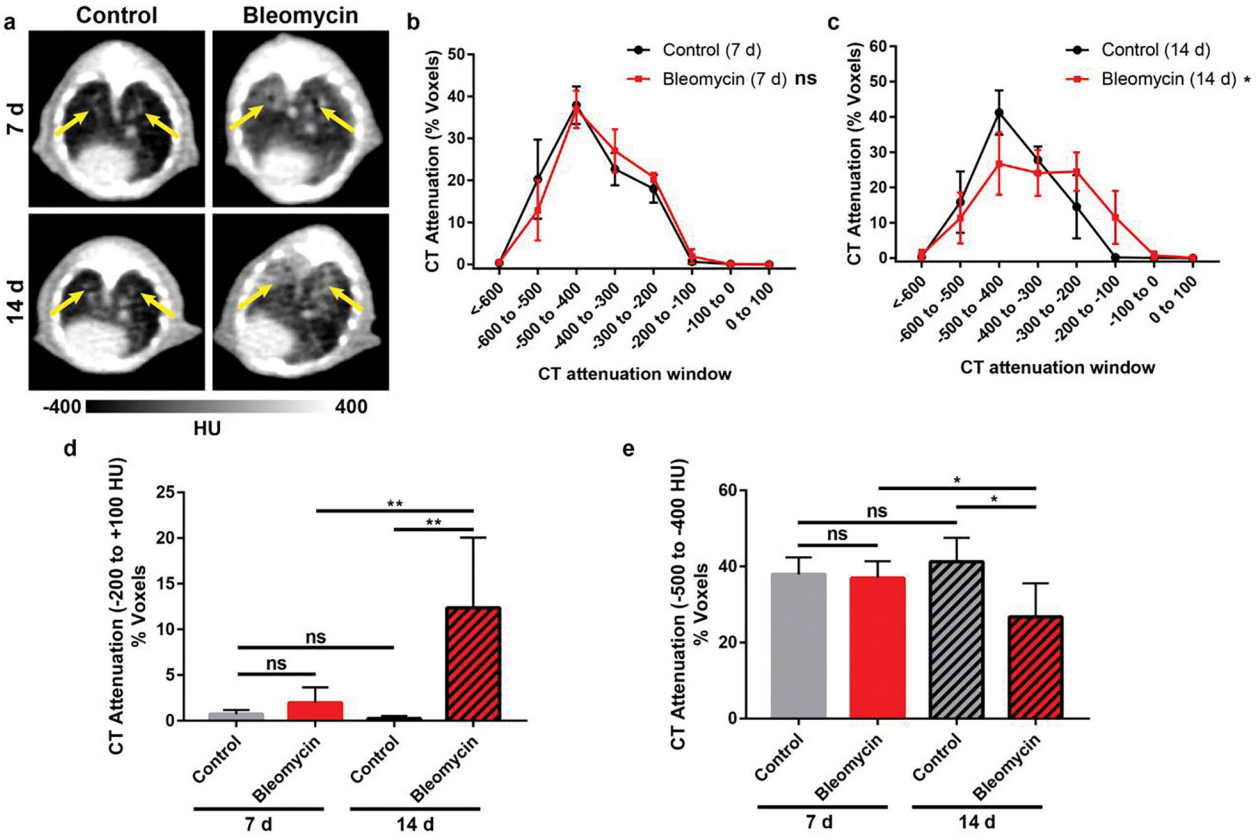

Figure 1.

Longitudinal CT imaging in a murine model of bleomycin-induced lung fibrosis. (**a**) Representative CT images of bleomycin and saline control mice at 7 d and 14 d following substance administration. Yellow arrows indicate lung volume (n = 5–7). CT attenuation voxel distributions of bleomycin and control mice at (**b**) 7 d and (**c**) 14 d post bleomycin. Groups were compared by Two-way ANOVA with Sidak's correction for multiple comparisons (* $P < 0.05$). Percentage of CT attenuation voxels were compared in the range of (**d**) −200 to + 100 HU to access extent of fibrosis and (**e**) −500 to −400 HU to assess lung aeration. CT only found differences between bleomycin and control mice at 14 d post instillation. P values were calculated using Student's two-tailed t-test (*P<0.05, **P<0.01).

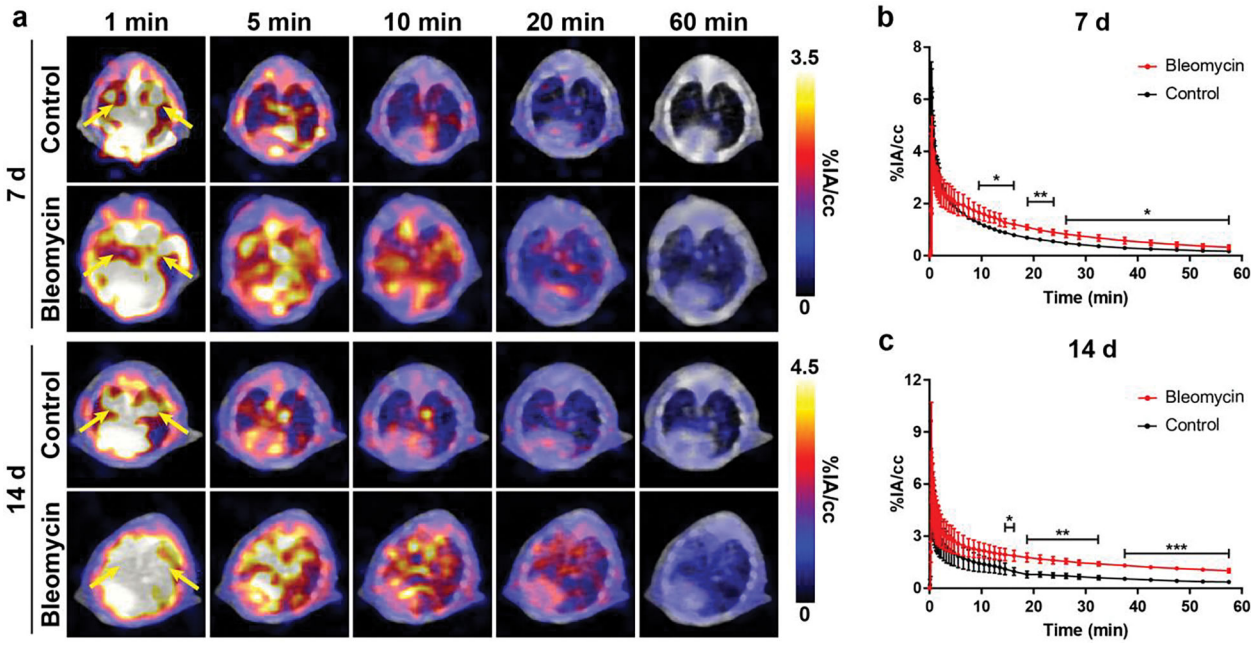

Figure 2.

Dynamic PET/CT using [^{68}Ga]Ga-FAPI-46 in a murine model of bleomycin-induced lung fibrosis. (**a**) Mice were intratracheally given bleomycin or saline as a control, and dynamic PET/CT was performed at 7 d and 14 d following bleomycin. Whole-lung time activity curves at (**b**) 7 d and (**c**) 14 d showed significantly higher uptake in injured lung vs. control, 15 min post-injection of [^{68}Ga]Ga-FAPI-46 (n = 3–5). Green arrows indicate lung volume. Lungs highlighted by yellow arrows. P values were calculated using Student's two-tailed t-test (*P<0.05, **P<0.01, ***P<0.001).

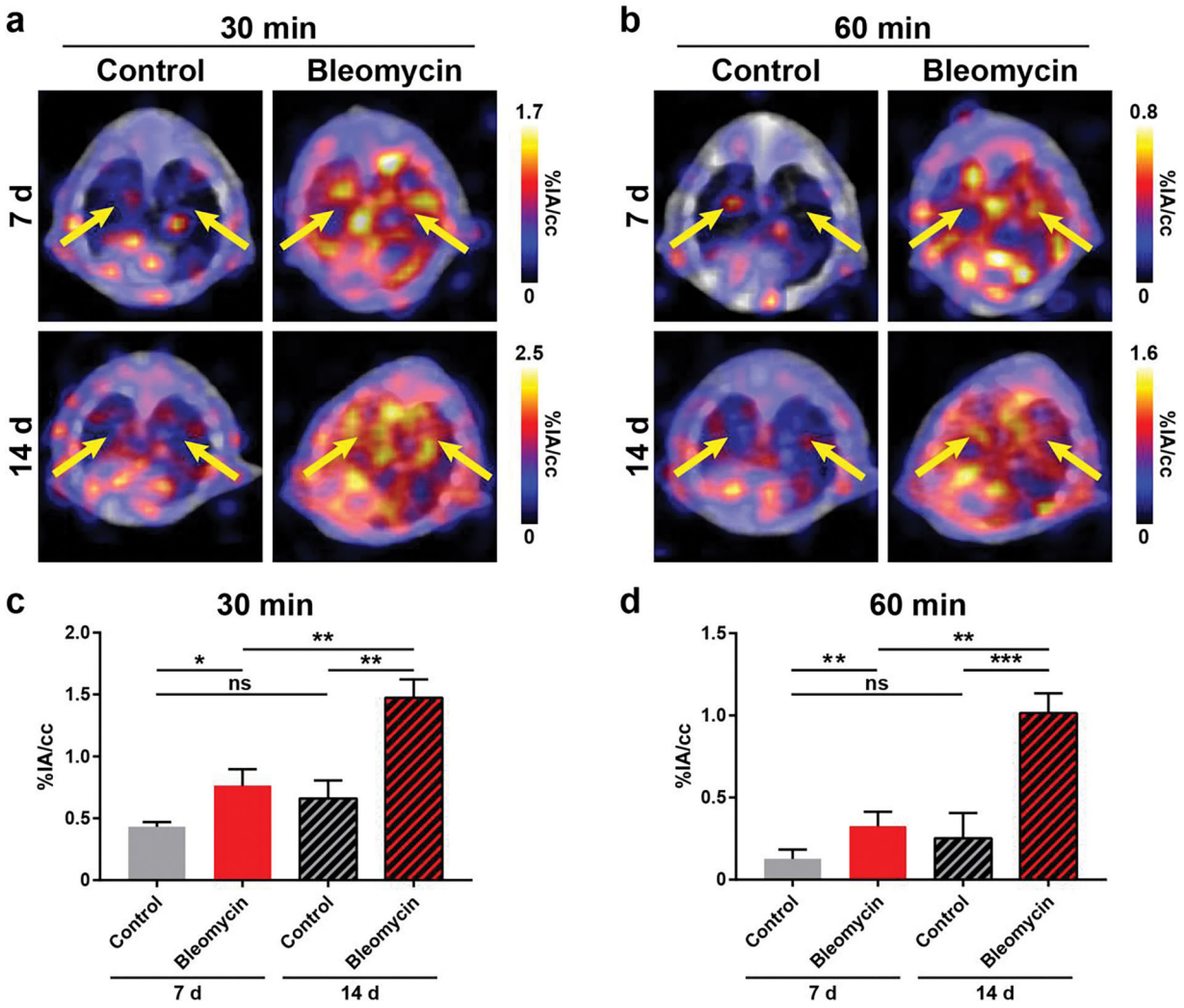

Figure 3.

Detection of activated fibroblasts with [^{68}Ga]Ga-FAPI-46 PET/CT in a murine model of bleomycin-induced lung fibrosis. PET/CT and VOI quantification of [^{68}Ga]Ga-FAPI-46 uptake in bleomycin and control mice found significantly higher [^{68}Ga]Ga-FAPI-46 uptake in the lungs of injured mice at (**a**, **c**) 30 min and (**b**, **d**) 60 min post-injection (n = 3–5). Lungs highlighted by yellow arrows. P values were calculated using Student's two-tailed t-test (*P<0.05, **P<0.01, ***P<0.001).

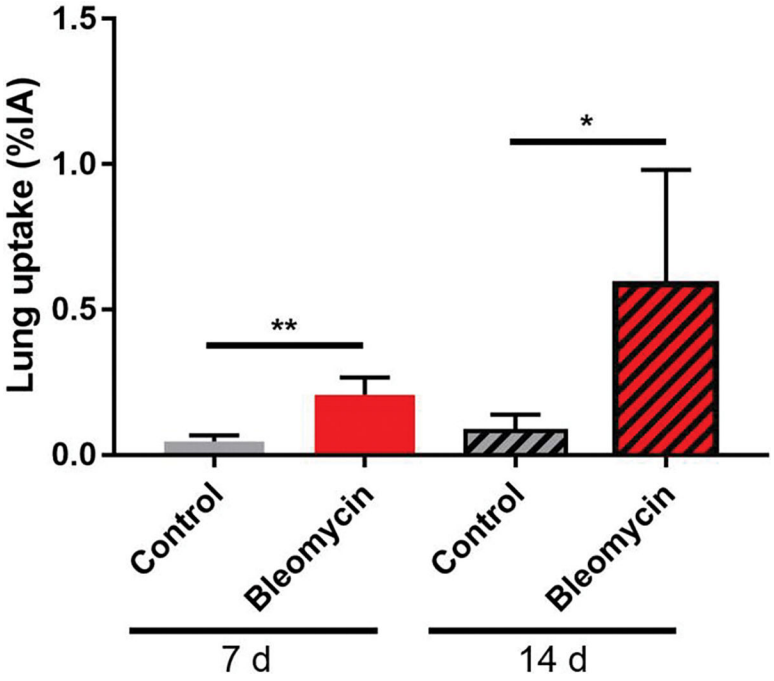

Figure 4.

Ex vivo biodistribution studies. Overall lung uptake was significantly higher in mice administered bleomycin compared to controls at both 7 d and 14 d following the procedure (n = 3–5). P values were calculated using Student's two-tailed t-test (*P<0.05, **P<0.01).

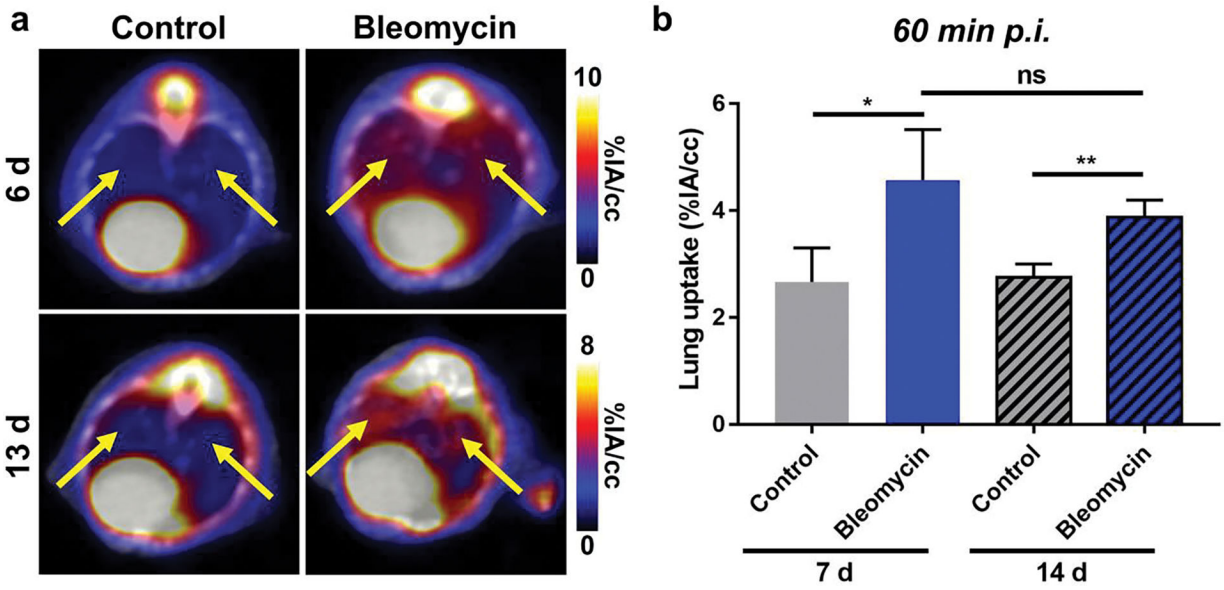

Figure 5.

[^{18}F]FDG PET/CT of pulmonary fibrosis. (**a**) PET/CT and (**b**) VOI quantification of [^{18}F]FDG in bleomycin and control mice found significantly higher lung uptake in injured mice at 60 min post-injection (n = 3–4) at 7 d and 14 d following pulmonary fibrosis induction. However, background was higher and lung uptake slightly decreased from 7 d to 14 d following bleomycin administration. Lungs highlighted by yellow arrows. P values were calculated using Student's t-test (*P<0.05, **P<0.01)

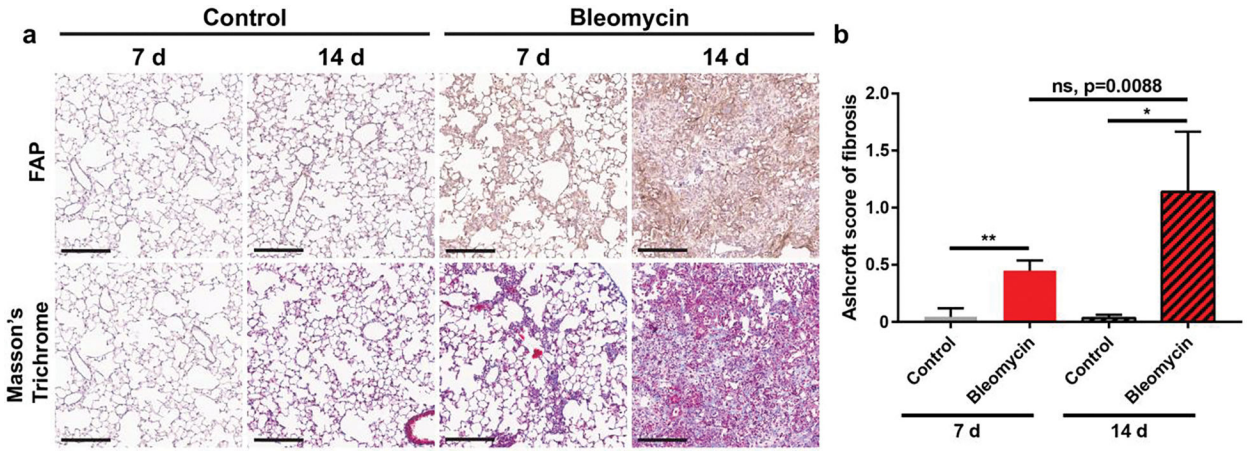

Figure 6.

Longitudinal histology of healthy lung and fibrotic lung. (**a**) Tissue staining revealed higher fibroblast activation protein expression and increased fibrosis in bleomycin injured mouse lung tissue than controls. Marked increase in both intensity and density of FAP expression and collagen deposition was observed between 7 d to 14 d post-bleomycin administration. Scale bar: 200 μm. (**b**) Ashcroft score of fibrosis for Masson's Trichrome staining of bleomycin administered and control mice. P values were calculated using Student's two-tailed t-test (*P<0.05, **P<0.01).